IEICE TRANS. ELECTRON., VOL.E87–C, NO.3 MARCH 2004

INVITED PAPER *Special Section on Photonic Crystals and Their Device Applications*

High Index-Contrast 2D Photonic Band-Edge Laser

Soon-Hong KWON[†a)] ***and*** **Yong-Hee LEE**[†]**,** ***Nonmembers***

SUMMARY Free-standing 2D slab photonic band-edge lasers based on square lattice and triangular lattice are realized by optical pumping at room-temperature. Both in-plane-emission and surface-emission photonic band-edge lasers are observed and compared. Analyses on optical loss mechanisms for finite-size photonic band-edge lasers are also discussed.

key words: *photonic crystal, semiconductor laser, band edge, in-plane emission, surface emission*

1. Introduction

Photonic crystals (PCs) have drawn much attention owing to their ability of photon control. Especially, the existence of the photonic bandgap (PBG), the frequency range in which the propagation of light is forbidden, opens various application areas as cavity quantum electrodynamics (QED) [1], low threshold lasers [2] and nano-waveguides [3]. Among multitudes of photonic crystal structures, two-dimensional (2D) photonic crystal slab structures are widely investigated, because they can be fabricated relatively easily by standard semiconductor fabrication processes. Especially, 2D slab photonic crystal lasers have demonstrated interesting feasibility as wavelength-scale coherent light sources [4]–[10]. Such photonic crystal lasers can be classified into two groups. One group that has a defect region shows lasing action around the localized cavity nearby the defect region by the photonic bandgap [4]–[6]. The other one does not have a physically defined cavity. As this type of photonic crystal lasers operates near the extremes of the photonic band, they are named as the photonic band-edge lasers [7]–[12]. In certain aspects, this type of the lasers can be interpreted as a 2D version of the conventional distributed feedback laser. Recently, various 2D photonic band-edge lasers have been demonstrated by several groups. In earlier versions of the band-edge laser [7]–[10], the effective refractive index-contrast has been very small and the device size was rather large to achieve the gain sufficient for lasing. Consequently, the laser threshold was usually high. However, in the high index-contrast structure [11], [12], lasing can be achieved in much smaller active area $\sim (10\times10\,\mu\mathrm{m})$ due to their reduced threshold gain. Such small band-edge lasers can be a good candidate for low-threshold and high-speed-modulation active devices.

In this paper, we describe characteristics of high index-contrast 2D photonic crystal band-edge lasers realized in the square lattice and the triangular lattice structure. The experimental data are analyzed by the three-dimensional (3D) plane wave expansion (PWE) method and the 3D finite difference time domain (FDTD) method. In Sect. 2, the photonic band-edge lasers are classified by the operating symmetry points in the k-space. Lasing characteristics, device fabrication, threshold behaviors, lasing wavelengths, near-field patterns and far-field patterns, and polarizations are described in Sect. 3. In Sect. 4, the emission and loss mechanisms of the lasing modes are analyzed through the comparison of the mode patterns in the real-space and the Fourier space.

Manuscript received September 1, 2003.
Manuscript revised October 31, 2003.

[†]The authors are with the Department of Physics, KAIST, Taejon, Korea.
a) E-mail: ksunong@kaist.ac.kr

2. Classification of Photonic Band-Edge Lasers

2.1 High Index-Contrast Air Slab Structure

At the band edges such as Γ, X, M (for square lattice structure) points, standing waves are formed by the superposition of reflected waves originating from the periodic index variation. Therefore, near these symmetry points, the group velocity of wave approaches zero and the density of photon states becomes infinity. If the group velocity becomes very slow, photons would have much longer time to interact with the active medium and experience the enhanced effective gain that is inversely proportional to the group velocity [13]. It is also well known that the group velocity near the band edges decreases with the index-contrast of the 2D slab. Therefore, the free-standing air slab structure to be discussed here is expected to be advantageous for the band-edge lasing operation because of its high index-contrast.

2.2 Symmetry Points at Photonic Band Edges

In order to explain the symmetry of the band-edge points, we use the photonic band diagram obtained by the 2D PWE method combined with the effective index approach because of the complexity of the band diagram obtained from the full 3D PWE method. Here, a refractive index 2.65 is used for the effective index of 2D PWE method. Therefore, the exact positions of the band edges are somewhat different from those of the 3D value. However, remember that the 3D PWE method is used to analyze the experimentally measured spectral data of the band-edge lasers in subsequent sections. The air hole radius, $0.35a$ is used. Figure 1 shows calculated photonic band diagrams of a triangular lattice

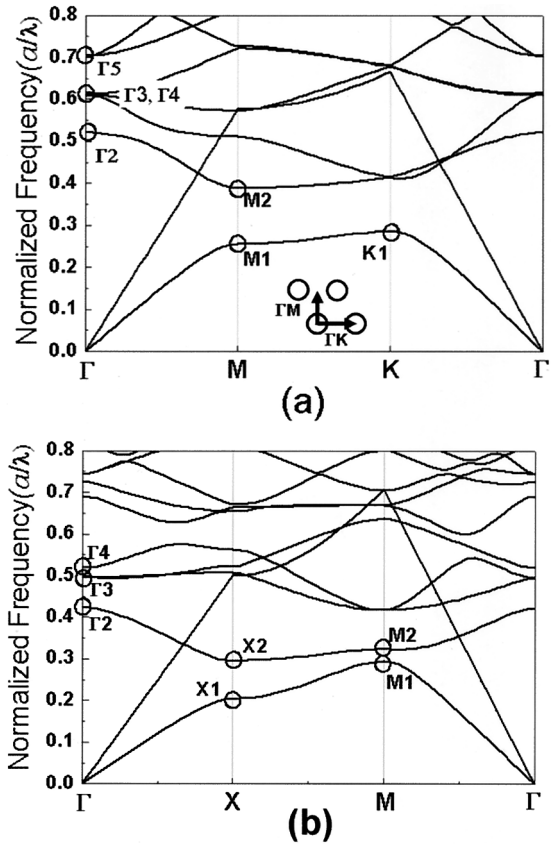

Fig. 1 Calculated band diagrams of (a) triangular lattice structure and (b) square lattice structure for TE mode by 2D PWE method. In the triangular lattice, Γ2 and Γ4 are non-degenerate modes, and Γ3 and Γ5 are doubly-degenerate modes [9]. In the square lattice, Γ3 is doubly-degenerate mode.

and a square lattice structure for the transverse-electric (TE) mode. Note that the dispersion curves are flat near the band edges that are represented as circles in Fig. 1. The photonic band-edge lasers can be classified into two groups by light lines. Those modes below the light lines are guided along the photonic crystal slab and the propagating modes above the light line are considered as leaky modes that couple easily into the free space out of slab. In fact, band-edge lasers operating below the light lines are well-guided by the slab as in the conventional waveguide structure. On the other hands at Γ points, although the modes are characteristically categorized as leaky modes since they are located above the light lines, these modes still do not couple with the radiation modes because of the mismatch of the spatial symmetry [14]. Therefore, the photon lifetime of the band-edge modes become infinite in an infinite 2D photonic crystal slab structure.

However, in practice, the size of the photonic crystal can not be infinite, and this finiteness results in unavoidable optical losses for the non-ideal band-edge modes. In a finite photonic crystal, the Block wave vector k is not a well-defined quantity since the translational symmetry is limited to the photonic crystal region. Therefore, the band-edge lasers operating at a finite photonic crystal can be

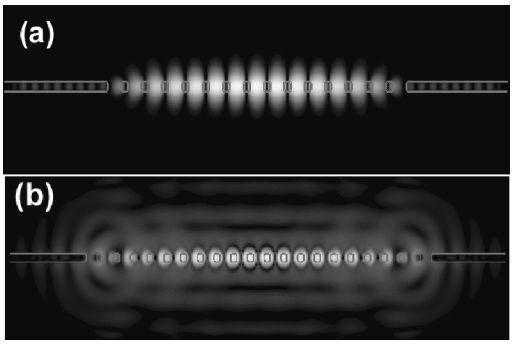

Fig. 2 Side views of the electric field intensity profiles in the (a) second X point band-edge laser of the square lattice structure and (b) second Γ point band-edge laser of the triangular lattice structure. Gray lines indicate the photonic crystal slab structures. Those are calculated by 3D FDTD method.

understood as the superposition of the modes with the k-components localized near the wave vector of the band-edges with some uncertainty (Δk). Since the modes except for the exact band-edge mode have the finite group velocities, the band-edge mode of a finite photonic crystal experiences optical losses into the in-plane direction of the slab. Through the 3D FDTD analyses of a finite 2D slab structure, it is found that the main loss mechanism of the band-edge modes below the light lines is the propagation of light into the un-patterned region of the slab as shown in Fig. 2(a). Since the major emission of this type of band-edge laser is into the in-plane direction, we call this laser as in-plane-emitting band-edge laser.

The Γ point band-edge lasers above light lines also have the in-plane loss similarly. However, there are additional non-negligible vertical couplings for the Γ point band-edge modes [9]. In fact, the vertical coupling to the free space out of the slab is forbidden by the symmetry mismatch [14] as previously mentioned. However, for finite size 2D slab structures, the uncertainty in the k-space allows vertical emission because the transverse wave vectors should be added to the vertical components of the modes and the symmetry mismatch condition is broken for such modes with those wave vectors. As a result, the modes near the Γ point tend to leak into the free space out of the slab, as is shown in Fig. 2(b). Here we call this type of the band-edge laser as surface-emitting band-edge laser.

3. Fabrication and Characteristics of 2D Photonic Band-Edge Laser

3.1 Fabrication

Typical schematic diagram of a free-standing slab structure is shown in Fig. 3(a). The active material consists of seven pairs of strain compensated InGaAsP quantum wells. Transverse magnetic (TM)-like modes are suppressed because of the compressive strain of the quantum wells. The maximum gain peak of the quantum well is at 1.55 μm. Air hole patterns are written on the PMMA by electron-beam lithogra-

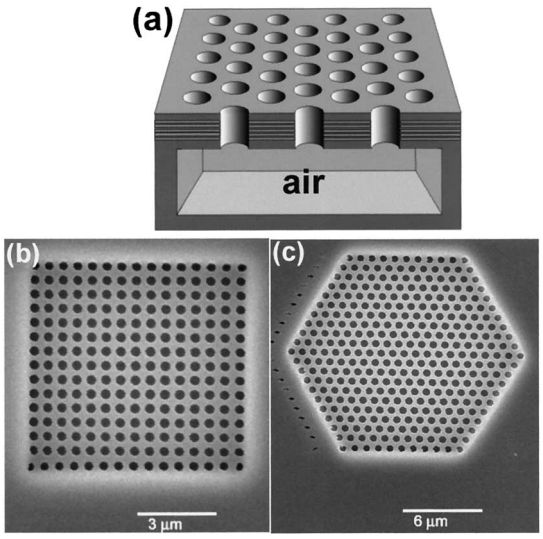

Fig. 3 (a) Schematic diagram of the band-edge laser in a free-standing slab structure. Scanning electron microscope images of the (b) square lattice and (c) triangular lattice.

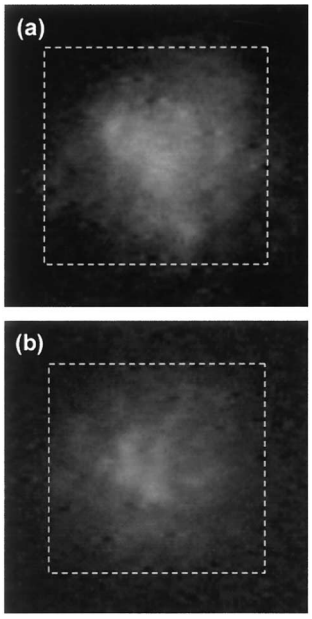

Fig. 4 Mode pattern images of (a) the second X and (b) the second M points band-edge lasers taken by a CCD camera. The dotted squares represent the boundaries of the photonic crystal lasers.

phy. After developing process, the ion milling using Ar gas hardens the PMMA. The patterns are transferred to the InP sacrificical layer that lies beneath the slab by Ar/Cl2 chemically assisted ion beam etching (CAIBE). Then the InP sacrificial layer is removed using a diluted HCl:H_2O (4:1) solution, and a free-standing structure are completed. The thickness of the resulting free-standing slab is 200 nm, which thus only supports the fundamental transverse electric (TE)-like mode. Figures 3(b) and (c) show scanning electron microscope images of the fabricated square lattice and triangular lattice photonic band-edge lasers, respectively. The photonic crystals consist of air holes (n=1.0) and InGaAsP (n=3.4). The lattice constants a of the square lattice structures are chosen to be in the range 450 to 600 nm to overlap the optical gain region with the second X (X2) and second M (M2) point band-edge lasers. The lattice constant of the triangular lattice for the Γ point band-edge lasing is found to be 874 nm. The radii of air holes also varies from $0.28a$ to $0.38a$. The number of air holes is 15×15 in the square lattice structure and 21×21 in the triangular lattice structure, and the side length of the square lattice samples is about 7.5 μm and that of the triangular lattice is about 17 μm.

The fabricated samples are pulse-pumped using a 980 nm laser diode at room temperature. The pumping beam is focused with a microscope objective lens (NA=0.85) and light emitted from the sample is collected by a charge-coupled device (CCD) and a monochromator with the same lens. The pulse width is 5 ns and the duty ratio is 0.25% so that the thermal effects on the photonic band-edge lasers become insignificant.

3.2 In-Plane-Emitting Band-Edge Laser: Square Lattice

In this section, we focused on in-plane-emitting band-edge lasers operating near the X2 and M2 point below the light line of the square lattice photonic crystal slab [17]. In general, triangular lattice photonic band-edge modes exhibit complicated 2D and 1D distributed feedback mechanisms [10]. On the other hands, the square lattice band-edge modes have relatively simple one-dimensional (1D) feedback mechanism. Therefore, the analyses of the square lattice band-edge modes are expected to be relatively more straightforward than those of triangular lattice band-edge modes. The lattice constants of the samples are 460 nm, 510 nm, and 550 nm. In the samples with those lattice constants, the X2 and M2 band-edge points fall well within the gain spectrum.

The near-field images of the X2 and M2 band-edge lasing are captured by a CCD camera, as shown in Fig. 4(a) and Fig. 4(b), respectively. The CCD images of these band-edge lasers are very weak and do not show any characteristic features contrary to the photonic crystal defect lasers or the surface-emitting band-edge lasers. In fact, most of the light escaped from the in-plane emitting band-edge lasers propagates along the slab out of the finite patterned region. In addition, it is interesting to note that one can not see the scattering at the boundaries of the photonic crystal patterns, even though the reflections of the guided modes are expected at the boundaries. This observation is also confirmed through the results of the FDTD computation, which show that the vertical mode profile in the photonic crystal region match very smoothly with those in the un-patterned region without the considerable scattering, as is shown in Fig. 2(a).

The variation of the measured normalized frequencies (plotted as dots) of the band-edge lasers with air-hole radius for each lattice constant are shown in Fig. 5(a) and Fig. 5(b). The normalized frequencies of the band-edge positions are

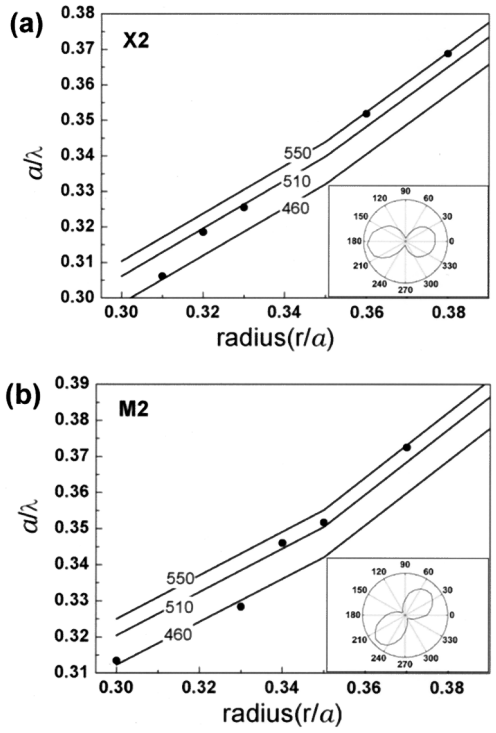

Fig. 5 The normalized frequency of (a) the second X and (b) second M band-edge lasers as a function of air-hole radius (r/a) for each lattice constant, 460 nm, 510 nm, and 550 nm. The dots represent the measured lasing positions of the band-edge lasers. Calculated band-edge frequencies at the second X, M by 3D PWE method are shown with lines. The insets of each figure indicate the measured typical polarization states of each band-edge lasers.

obtained by the 3D PWE method and are represented by the lines in Fig. 5. The calculated frequencies of the X2 and M2 band edges agree closely with the observed spectral positions for each lattice constant and air-hole radius. The slight discrepancies between the experimental and calculated results are believed to be originated from structural imperfections and errors in the measurement of the lattice constant and the air-hole radius. In addition, the frequencies of the X2 and M2 band-edges are very close to each other, as shown in Fig. 1(a). Thus, measurement of the lasing wavelengths is not sufficient to identify the lasing modes.

In order to confirm the identifications of the lasing modes, the polarization states are investigated for each band-edge laser. In the case of the X and M point band-edge modes, there are two equivalent lasing oscillation pairs consisting of two wave vectors having opposite directions. The X2 mode has the lasing oscillation directions along the 0 degrees (x-direction) and 90 degrees (y-direction) with respect to the boundary of the sample. However, these oscillations will be split if the 4-fold symmetry is broken by structural asymmetry. Therefore, either x-directional or y-directional lasing oscillation is preferred in real situation. Then either y-directional or x-directional linear polarization orthogonal to the oscillation direction is observed, as shown in the inset of Fig. 5(a). In the case of the M2 mode, similar analyses can be applied: the polarization direction of either +45 degrees

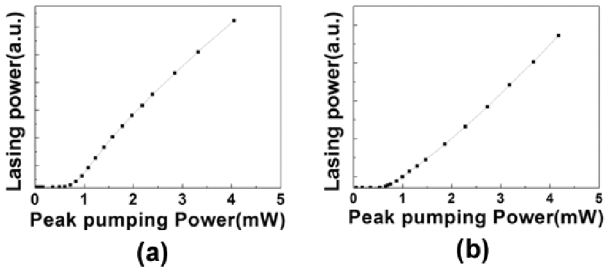

Fig. 6 Collected powers at the lasing wavelength is plotted for (a) the second X and (b) second M band-edge lasers as a function of incident peak pump power.

or −45 degrees is observed as shown in the inset of Fig. 5(b). In other words, the lasing modes with the polarization direction parallel to the boundaries of the photonic crystal pattern corresponds to the second X band-edge mode, and the lasing modes with the polarization direction diagonal to the boundaries of the pattern correspond to the second M band-edge mode. The identification of the polarization state unambiguously differentiates the X2 laser modes from the M2 band-edge laser modes, for all samples with lattice constants in the range from 400 nm to 600 nm.

Figure 6 shows the collected power at the lasing wavelength as a function of incident peak pump power for the typical second X and second M band-edge lasers. The threshold peak pump powers of the X2 and M2 band-edge lasers are ~ 0.67 mW and ~0.62 mW, respectively, with a pumping spot size of ~4 μm. These threshold values are very low compared to that of the first K point triangular band-edge lasers [12]. The threshold of the first K point triangular band-edge laser with silica cladding was reported bigger than 3 mW. The calculated large quality factors (Q) of 1100 and 8700 of the X2 and M2 modes are partly responsible for the low threshold behaviors. For comparison, the calculated quality factor in our FDTD simulation is only 350 for the first K point triangular lattice band-edge mode of a slab structure with silica cladding.

3.3 Surface-Emitting Band-Edge Laser

In the low-index contrast structure, the Γ point band-edge lasers reported the diffraction-limited divergence angles [9], [10]. Since such structures need relatively large photonic crystal areas for band-edge lasing, the number of the air holes participating in the lasing actions is much larger than that of the high index-contrast structure. As the number of air holes of the photonic crystal patterns increases, the wave vector is well determined in the proximity of the Γ point so that the vertical emission with very low divergence angle can be possible. On the other hands, we observed the interesting emission characteristics from the high index-contrast triangular lattice structure with 21 rows of air holes through the far-field measurement setup explained in Ref. [15]. The fabricated samples are pulse-pumped by a 980 nm laser diode placed at the backside of the sample so that the laser does not disturb the far-field measurement.

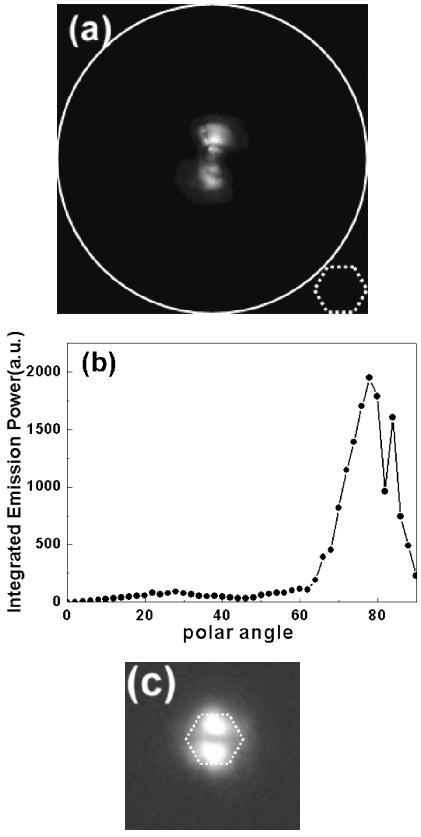

Fig. 7 Typical lasing characteristics of the Γ point band-edge laser. (a) The far-field image of the band-edge laser measurement. The center of the image corresponds to the vertical direction. The circle indicates the horizontal direction and the dotted hexagon represents the direction of the sample. (b) The integrated radiation over the azimuthal angle is plotted as a function of the polar angle. Maximum is positioned not at the 90 degree, but at the 76 degree. (c) The CCD image of the band-edge laser. The dotted hexagon represents the sample boundaries.

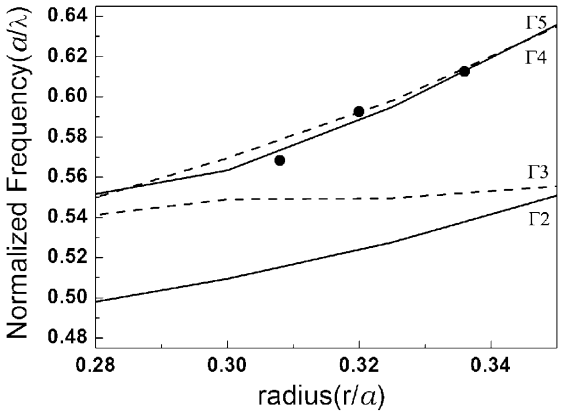

Fig. 8 The normalized frequency of the Γ point band-edge laser as a function of air-hole radius (r/a) for lattice constant, 874 nm. The closed circles represent the measured lasing positions of the band-edge lasers. From the lower frequency, the calculated second Γ(Γ2) third Γ(Γ3) fifth Γ(Γ5), fourth Γ(Γ4) point band-edges by 3D PWE method are shown with lines. Non-degenerate modes (Γ2, Γ4) and doubly-degenerate modes (Γ3, Γ5) correspond to the dashed lines and the solid lines, respectively. The spectral positions of the Γ4 and Γ5 band-edges are very close to each other.

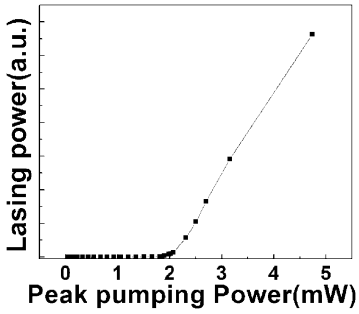

Fig. 9 Collected powers at the lasing wavelength is plotted for the fourth Γ point band-edge laser.

The backside of the sample is polished to reduce the scattering losses. The photodetector is placed 30cm from the sample. The angular resolutions of the azimuthal and polar direction are 9° and 2°, respectively. The far-field profile is shown in Fig. 7(a). The measured far-field pattern over the virtual hemisphere with the 30 cm radius is projected onto a flat surface. The center of the 2D flat surface corresponds to the vertical direction with respect to the sample surface. Note that most of the radiation energy falls within ±30°, as shown in Fig. 7(b). This observation demonstrates vertical emission characteristics of the Γ point band-edge laser. Interestingly, we observed the intensity minimum along the vertical direction, as shown in Figs. 7(a) and (b). This can be explained only when the coupling of the Γ point band-edge modes with the free space modes are forbidden along the exact vertical direction. In addition, the two opposite directional pairs of the far-field lobes are placed near the vertical direction in Fig. 7(a) and two bright spots in the CCD near-field image of Fig. 7(c) are placed along the two opposite ΓX directions. We believe that the small imperfection of the sample, such as slight elongation of the air holes and misplacement of the air holes are responsible for this observation of the far-field emission patterns.

The measured wavelength from the samples with lattice constant of 874 nm ranges from the 1420 nm to 1540 nm depending on the air hole radii. The spectral positions correspond to the normalized frequencies of the Γ4 and Γ5 point band edges, as shown in Fig. 8. On the other hands, Γ2, Γ3, Γ4 and Γ5 band-edge modes have the symmetry reminiscent of hexapole, doublely-degenerate quadrupole, monopole, and doubly-degenerate dipole modes, respectively [9].

And those Γ point band-edge modes are classified into B2, E2, A1, and E1 symmetry groups by the group theory notation [14]. Since the mode propagating in free space with vertical wave vector has E1 symmetry, the B2 (Γ2), E2 (Γ3), and A1 (Γ4) band-edge modes except for the E1 (Γ5) mode are not allowed to be couple into the free space because of the symmetry mismatch. The alternative possibility is that the Γ5 band-edge mode is a fully leaky mode and very lossy. In fact, we are unable to separate this resonance in our FDTD computation. Therefore, it is more likely that the lasing bane-edge mode corresponds to the Γ4 mode.

The measured threshold peak pump power of one of the fourth Γ point band-edge laser is ~ 2.1 mW, as is shown in Fig. 9, which indicates this lasing mode has considerably large optical loss. The calculated quality factor of the Γ4 mode for this structure is indeed only 550.

4. Analysis of Lasing Mode

4.1 Analysis of Polarization and Emission Characteristics of In-Plane Emitting Band-Edge Lasers

In order to understand the characteristics of the in-plane-emitting band-edge lasers, calculations are carried out for finite structures with the 3D FDTD method. Figure 10(a) shows the calculated electric field intensity profile of the X2 band-edge mode oscillating in the y-direction. One can select one mode between two X2 modes applying symmetric conditions in the FDTD calculation. The transformation of this real-space mode pattern into the Fourier space is shown in Fig. 10(b). As is expected in Fig. 10(a), most of the guided modes are localized near the upper and bottom X points in the k-space and this fact explains the mode oscillation along the y-direction. The field components with these two opposing wave vectors form standing waves inside the photonic crystal pattern, and the photons corresponding to the standing waves have almost zero group velocity. On the other hands, the light propagation out of the structure is explained again as finite-size effect [16]. The wave vectors not localized at exact X points form quasi-standing waves which have the nonzero group velocity along the y-direction.

In addition, the components in the light line indicated by white circle in Fig. 10(b), which result from the spreading of wave vectors, are able to couple with the free space propagating modes. However, remember that these components are much smaller than the in-plane loss. Therefore, the in-plane-emitting band-edge laser emits mostly along and inside the slab and very small amount of the energy are emitted out of the slab. Naturally, most of the photons emitted into the free space have the y-directional wave vectors and the state of the polarization becomes the x-directional linear polarization. This is indeed confirmed in the inset of the Fig. 5(a). The diagonal-directional linear polarization of the M2 band-edge mode shown in the inset of Fig. 5(b) can also be explained in a similar manner by the FDTD analyses.

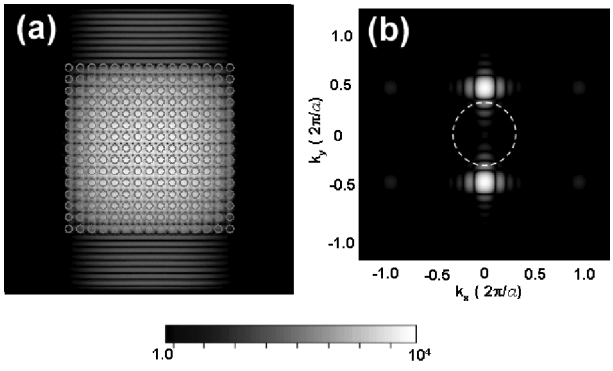

Fig. 10 (a) Top view of the electric field intensity profile of the second X point band-edge mode. The gray circles represent the air holes. (b) Fourier space field pattern of the second X point band-edge mode. The dotted circle indicates the light cone. Both the slab thickness and air-hole radius are 0.35*a*, the number of rows of air holes is 15.

4.2 Analysis of Emission Characteristics of Surface-Emitting Band-Edge Lasers

In order to investigate the emission characteristics of the Γ point band-edge lasers, far-field patterns are calculated through the Fourier transformation of the electric field and the magnetic field components parallel to the surface of the photonic crystal, in which the field components are obtained by the 3D FDTD method [18].

Figure 11 shows the calculated far-field patterns for the Γ4 band-edge mode for the samples of different sizes. General features agree well with the experimental result. Major radiation is directed along the near-vertical direction, and the true vertical emission is not observed in Fig. 11. In addition, the divergence angle of the Γ point band-edge mode becomes smaller as the number of air holes increases. On the other hands, in the Fourier space, wave vectors are localized in the proximity of the six nearest Γ points and at the origin (the fundamental Γ point placed inside light cone), as shown in Fig. 12. As is expected, the photons with wave vectors inside the light cone are non-negligible and the wave vectors have relatively small transverse components. In other words, if one sees carefully the center of k-space mode patterns, there exists very small opening inside k-space localization. This node demonstrates the impossibility of the exact vertical emission, which is related to the symmetry mismatch in the k-space. On the other hands, it is directly observed that uncertainty of k-space decreases as the photonic crystal size increase.

Additionally, if the six-fold symmetry is broken, the coupling strengths to the each Γ point would be different. However, the standing waves can still be form if the structure has some mirror symmetry as in the case of the y-directional or x-directional elongated structure. In such cases, two or four opposing Γ wave vectors can construct standing waves when those wave vectors are balanced with

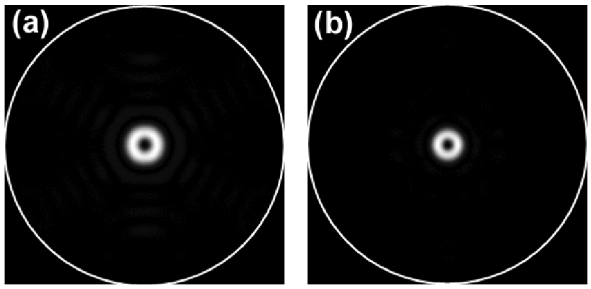

Fig. 11 Calculated far-field patterns of the fourth Γ point band edge modes in the case of samples with (a) N~17 and (b) N~21. Here, the size parameter N corresponds to the number of air holes along the ΓK direction at the center of the pattern.

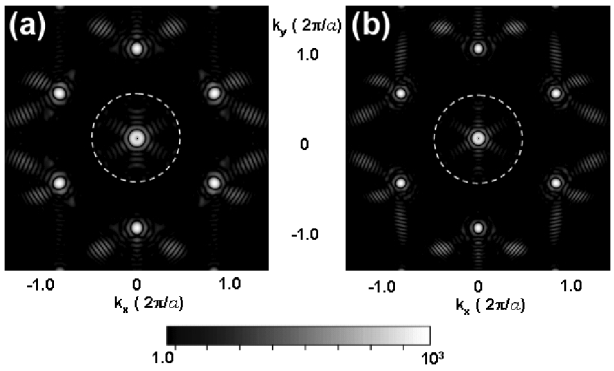

Fig. 12 Fourier space field patterns of the fourth Γ point band-edge mode in the case of the samples with (a) N∼17 and (b) N∼21. The circle indicates the light cone. Six bright spots outside the light cone correspond to the nearest Γ points. All spots in the case of the structure of N∼21 are smaller than those in the case of the structure of N∼17.

each other. The two lobes observed in the far-field measurement are believed to have the origin of those reasons. In fact, the directions of the lobes correspond to the two opposite Γ direction.

5. Conclusion

We have demonstrated the lasing oscillation of a 2D photonic crystal lasers in high index-contrast photonic crystal slab and have classified them into two groups according to the emission direction. Operation points of in-plane-emitting square lattice band-edge lasers are identified as the second X band-edge point or second M band-edge point through the measurement of the spectral position and the polarization direction. This confirmation agrees well with theoretical calculations by the 3D PWE method and the 3D FDTD method. The main direction of the optical losses of the in-plane emission device is found to be horizontal rather than vertical. For triangular lattice surface-emitting photonic band-edge lasers operating near the Γ-point, it is interesting to report that the emission into the exact vertical direction is not observed. This observation can be explained by the symmetry argument.

Acknowledgments

This work was supported by the National Research Laboratory Project and Nano Research & Development Program of KISTEP, Korea.

References

[1] J. Vuckovic, M. Loncar, H. Mabuchi, and A. Scherer, "Design of photonic crystal microcavities for cavity QED," Phys. Rev. E, Stat. Phys. Plasmas Fluids Relat. Interdiscip. Top., vol.65, pp.016608-1–11, 2001.

[2] H.G. Park, J.K. Hwang, J. Huh, H.Y. Ryu, Y.H. Lee, and J.S. Kim, "Nondegenerate monopole-mode two-dimensional photonic band gap laser," Appl. Phys. Lett., vol.79, pp.3032–3034, 2001.

[3] M. Loncar, D. Nedeljkovic, T.P. Perasall, J. Vuckovic, A. Scherer, S. Kuchinsky, and D.C. Allan, "Experimental and theoretical confirmation of Bloch-mode light propagation in planar photonic crystal waveguides," Appl. Phys. Lett., vol.80, pp.1689–1691, 2002.

[4] J.K. Hwang, H.Y. Ryu, D.S. Song, I.Y. Han, H.W. Song, H.G. Park, Y.H. Lee, and D.H. Jang, "Room-temperature triangular-lattice two-dimensional photonic band gap lasers operating at 1.54 μm," Appl. Phys. Lett., vol.76, pp.2982–2984, 2000.

[5] O. Painter, R.K. Lee, A. Scherer, A. Yariv, J.D. O'Brien, P.D. Dapkus, and I. Kim, "Two-dimensional photonic band-gap defect mode laser," Science, vol.284, pp.1819–1821, 1999.

[6] M. Loncar, T. Yoshie, A. Scherer, P. Gogna, and Y. Qiu, "Low-threshold photonic crystal laser," Appl. Phys. Lett., vol.81, pp.2680–2682, 2002.

[7] M. Imada, S. Noda, A. Chutinan, T. Tokuda, H. Kobayashi, and G. Sasaki, "Coherent two-dimensional lasing action in surface-emitting laser with triangular-lattice photonic crystal structure," Appl. Phys. Lett., vol.75, pp.316–318, 1999.

[8] M. Meier, A. Mekis, A. Dodabalapur, A. Timko, R.E. Slusher, J.D. Joannopoulos, and O. Nalamasu, "Laser action from two-dimensional distributed feedback in photonic crystals," Appl. Phys. Lett., vol.74, pp.7–9, 1999.

[9] M. Imada, A. Chutinan, S. Noda, and M. Mochizuki, "Multidirectionally distributed feedback photonic crystal lasers," Phys. Rev. B, Condens. Matter, vol.65, pp.195306-1–8, 2002.

[10] M. Notomi, H. Suzuki, and T. Tamamura, "Directional lasing oscillation of two-dimensional organic photonic crystal lasers at several photonic band gaps," Appl. Phys. Lett., vol.78, pp.1325–1327, 2001.

[11] H.Y. Ryu, S.H. Kwon, Y.J. Lee, Y.H. Lee, and J.S. Kim, "Very-low-threshold photonic band-edge lasers from free-standing triangular photonic crystal slabs," Appl. Phys. Lett., vol.80, pp.3476–3478, 2002.

[12] C. Monat, C. Seassal, X. Letartre, P. Regreny, P. Rojo-Romeo, P. Viktorovitch, M.L. Vassor, D'Yerville, D. Cassagne, J.P. Albert, E. Jalaguier, S. Pocas, and B. Aspar, "InP-based two-dimensional photonic crystal on silicon: In-Plane Bloch mode laser," Appl. Phys. Lett., vol.81, pp.5101–5104, 2002.

[13] J.P. Dowling, M. Scalora, M.J. Bloemer, and C.M. Bowden, "The photonic band edge laser: A new approach to gain enhancement," J. Appl. Phys., vol.75, pp.1896–1899, 1994.

[14] K. Sakoda, Optical Properties of Photonic Crystals, Springer-Verlag, Berlin Eidelberg, 2001

[15] D.J. Shin, S.H. Kim, J.K. Hwang, H.Y. Ryu, H.G. Park, D.S. Song, and Y.H. Lee, "Far- and near-field investigations on the lasing modes in two-dimensional photonic crystal slab lasers," IEEE J. Quantum Electron., vol.38, pp.857–866, 2002.

[16] H.Y. Ryu, M. Notomi, and Y.H. Lee, "Finite-difference time-domain investigation of band-edge resonant modes in finite-size two-dimensional photonic crystal slab," Phys. Rev. B, Condens. Matter, vol.68, pp.045209-1–9, 2003.

[17] S.H. Kwon, H.Y. Ryu, G.H. Kim, Y.H. Lee, and S.B. Kim, "Photonic bandedge lasers in two-dimensional square-lattice photonic crystal slabs," Appl. Phys. Lett., vol.83, pp.3870–3872, 2003.

[18] J. Vuckovic, M. Loncar, H. Mabuchi, and A. Scherer, "Optimization of the Q factor in photonic crystal microcavities," IEEE J. Quantum Electron., vol.38, pp.850–856, 2002.

Soon-Hong Kwon received the B.S. and M.S. degrees in 1999 and 2001, respectively, from the Department of Physics, Korea Advanced Institute of Science and Technology (KAIST), Taejon, where he is working toward the Ph.D. degree. His research interest include design, fabrication, and characterization of photonic crystal light-emitting structures.

Yong-Hee Lee received his master degree in Applied Physics and the Ph.D. degree in Optical Sciences at Korea Advanced Institute of Science and Technology in 1979 and at the University of Arizona in 1986, respectively. After the Ph.D., he joined AT&T Bell Laboratories at Holmdel, New Jersey. During his stay at AT&T Bell Laboratories, he demonstrated the first proton-implanted VCSELs in 1990 and holds the original patent on this industrial VCSEL. He has continued his research on VCSELs after he joined the Department of Physics of KAIST in 1991. Recently, his main interest lies in thresholdless photonic bandgap lasers and nano-photonic integrated optical circuits. He was elected as the recipient the IEEE LEOS Distinguished Lecturer Award for 2003–2004. He has co-authored over 90 international journal papers and patent related to VCSELs and photonic bandgap structures.